*Electronic Supplementary Information*

# Electrosynthesis, Functional, and Structural Characterization of a Water-Oxidizing Manganese Oxide

**Ivelina Zaharieva,*[a] Petko Chernev,[a] Marcel Risch,[a, c] Katharina Klingan,[a] Mike Kohlhoff,[a] Anna Fischer,[b] and Holger Dau*[a]**

[a] *Fachbereich Physik, Freie Universität Berlin, Arnimallee 14, 14195 Berlin, Germany.*

*E-mail: ivelina.zaharieva@fu-berlin.de; holger.dau@fu-berlin.de;*

*Fax: +49 30 838 56299; Tel: +49 30 838 53581*

[b] *Institute of Chemistry, Technical University Berlin, Straße des 17. Juni, 10623 Berlin, Germany*

[c] *present address: Electrochemical Energy Laboratory, MIT, 77 Massachusetts Ave, Cambridge, MA-02139, USA*

## S-1. Details of experimental procedures

**A. Electrodeposition.** Reagents: $(Mn(CH_3COO)_2 \cdot 4H_2O$ (Fluka, ≥99%), $H_2KPO_4$ (Roth, ≥99%), $K_2HPO_4$ (Roth, ≥99%), $MgSO_4 \cdot 7H_2O$ (AppliChem, ≥99.5%), $Na(CH_3COO)$ (Sigma-Aldrich, ≥99%), $CH_3COOH$ (AppliChem, 100%), $MnCl_2 \cdot 4H_2O$ (Roth, ≥98%), $Mg(CH_3COO)_2 \cdot 4H_2O$ (Fluka, 99%), $MnSO_4 \cdot 4H_2O$ (Merck, p.A.), $NaClO_4$ (Aldrich, 99.99% trace metal basis), $Co^{II}(OH_2)_6(NO_3)_2$ (Sigma Aldrich, ≥99.9%), $Ni^{II}(OH_2)_6(NO_3)_2$ (ChemPur, ≥99%), $H_3BO_3$ (Merck, p.A.), KOH (Sigma Aldrich, ≥86%). All reagents where used without further purification. Solutions were prepared with 18 MΩ·cm Milli-Q water. The electrochemical experiments were performed at room temperature using a potentiostat (SP-300, BioLogic Science Instruments) controlled by EC-Lab v10.20 software package. The Mn films were deposited in de-ionised water, in 0.1 M $MgSO_4$ or in 0.1 M Na acetate buffer (pH 6.0). If not stated otherwise, Mn(II) acetate tetrahydrate in final concentration of 0.5 mM was added as a source of $Mn^{2+}$ ions.

The conditions for electrodeposition were kept as simple as possible. The solutions were not stirred during the experiments, and if not stated otherwise, also not dearated. A single-compartment three-electrode electrochemical cell was used with saturated $Hg/Hg_2SO_4$ electrode (RE-2C, BioLogic) as reference electrode and a platinum mesh as counter electrode. The working electrode was 2 $cm^2$ (2 cm × 1 cm) indium-tin oxide (ITO) coated glass plate, 8-12 Ω/sq (purchased from Sigma-Aldrich). The volume of the solution was 100 mL. The pH was adjusted using 3 M NaOH only for the buffered systems (0.1 M phosphate or 0.1 M acetate buffer). The pH of the other solutions used for film deposition was typically between 6 and 6.5 (which did not affect the reproducibility) and was not adjusted.

For comparison of the turnover frequency (TOF), catalytically active Co and Ni oxides were electrodeposited, The Co oxide was deposited at constant potential in 0.1 M phosphate buffer as described in ref.[1], but using an anode potential of +1.05 V (*vs.* NHE) which is below onset of catalytic activity. The total charge during the electrodeposition was used to estimate the amount of deposited Co ions (assuming that $Co^{2+}$ gets oxidized to $Co^{3+}$ during the deposition). Oxygen evolution was measured as described in S-1C applying a constant potential of 1.35 V at pH 7 in Co-free 0.1 M phosphate buffer. The Ni oxide was deposited at constant potential in 0.1 M borate buffer at pH 9.2 as described in refs.[2-3] At the deposition potential of 1.15 V the catalytic current was still small. The charge during the deposition was used to estimate the amount of the deposited Ni, assuming change of oxidation state of Ni from +2 in the solution to +3 in the deposited material. Oxygen evolution was measured in Ni-free borate buffer (0.1 M) at pH 9.2.

**B. UV-vis spectroscopy.** UV-vis measurements were performed using Varian Cary 50 UV-vis spectrophotometer. To realize in situ measurements, a modified quartz cuvette (2.5 cm × 2.5 cm × 4 cm height) filled with 15 ml electrolyte was placed in the optical compartment of the spectrometer. The transparent working electrode was placed in front of the detector window and the $Hg/Hg_2SO_4$ reference electrode (5 mm diameter) and the platinum counter electrode were placed next to the walls of the cuvette in such a way that they were not hit be the measuring beam. The electrochemistry was controlled by a potentiostat (SP-300). For the spectrum of the inactive film shown in Fig 2, a slightly negative value was detected at the absorption minimum because of minor imprecision in the baseline determination.

**C. Detection of $O_2$ evolution.** The oxygen evolution was measured with a Clark-type electrode, (liquid-phase oxygen electrode chamber DW1, Hansatech Instruments). The counter, working, and reference electrodes of the electrochemistry setup were inserted into the solution compartment of the oxygen electrode chamber. The counter electrode (platinum mesh) was wrapped around the glass tube of the reference $Hg/Hg_2SO_4$electrode. The working electrode was an ITO-coated glass plate (0.5 cm × 1 cm). The contact between the ITO surface and the potentiostat cable was secured by copper tape, which was isolated from the solution by parafilm. The cell was filled with 3 ml 0.1 M phosphate buffer (pH 7) and sealed with a rubber ring and parafilm, leaving no gas phase volume. To remove the $O_2$ from the buffer solution, nitrogen gas was bubbled through the solution, for several minutes, before complete sealing of the Clark cell. The Clark cell was calibrated using $O_2$-free water and $O_2$-saturated water. The signal was recorded with a computer using a digital oscilloscope (Voltcraft® DSO-2090 USB).

In control experiments, we verified that the Clark electrode for polarographic detection of dioxygen does not interfere with the electrochemical experiment. To ensure interference-free function, the electronics used for detection of the $O_2$-reduction current and application of the polarization voltage (-0.7 V) to the platinum cathode and silver anode was completely galvanically insulated from the electrochemical set up. The two Clark-cell electrodes were covered with a KCl solution (3 M) and separated from the buffer solution by a diaphragm permeable only to dioxygen. Switching on and off the anodic potential (i.e. 1.35 V) on the potentiostat did not change the $O_2$ signal (with bare ITO electrode). Also switching on and off the polarization voltage of the Clark cell did not change the (catalytic) current recorded when a constant potential of 1.35 V was applied to the MnCat in the Clark-cell.

**D. SEM images and elemental analysis.** Scanning electron microscopy (SEM) and energy-dispersive X-ray analysis (EDX) were performed with a JEOL 7401F scanning electron microscope operated at 10 kV and equipped with a Bruker Quantax 400 EDX detector.

Elemental analysis was done using the PicoFox Spectrometer (Bruker) for total reflection X-ray fluorescence (TXRF) measurements. The Mn oxide films that had been deposited on 1 $cm^2$ ITO coated glass plate were dissolved in 500 µl of 30% HCl by exposing the films to the acid for several minutes. 100 µl of the resulting solution were mixed with 100 µl of a solution containing a Ga standard ($Ga(NO_3)_3$, concentration of 10 mg/l), and 5 µl of the mixture were deposited on a silicon-coated quartz glass sample plate. The acquisition time was 30 min per sample.

**E. XAS measurements and simulations.** X-ray absorption spectroscopy at the *K*-edge of manganese was performed at the KMC-1 beamline at the BESSY synchrotron (Helmholtz-Zentrum Berlin, Germany) at 20 K in a liquid-helium cryostat as described elsewhere.[4] Spectra were recorded in fluorescence mode using a 13-element Ge detector (Canberra). The extracted spectrum was weighted by $k^3$ and simulated in *k*-space ($E_0$ = 6547 eV). All EXAFS simulations were performed using in-house software (SimX3) after calculation of the phase functions with the FEFF program[5-6] (version 8.4, self-consistent field option activated). Atomic coordinates of the FEFF input files were generated for several reasonable structural models; the EXAFS phase functions did not depend strongly on the details of the used model. An amplitude reduction factor $S_0^2$ of 0.7 was used. The data range used in the simulation was 20–1000 eV (3–16 $Å^{-1}$). The EXAFS simulation was optimized by a minimization of the error sum obtained by summation of the squared deviations between measured and simulated values (least-squares fit). The fit was performed using the Levenberg-Marquardt method with numerical derivatives. The error ranges

of the fit parameters were estimated from the covariance matrix of the fit, and indicate the 68 % confidence intervals of the corresponding fit parameters. The fit error was calculated as in ref.[3]

For XAS samples preparation, mostly 1.35 V was applied for 2 min in a Mn-free phosphate buffer (pH 7). After that the samples were quickly taken out of the solution, rinsed with de-ionized water and frozen in liquid nitrogen where they were kept until the XAS measurements. To verify that during rinsing and freezing of the sample there is no major change in the structure, we prepared samples according to a procedure detailed in the following which allows freezing of the MnCat in liquid nitrogen under applied potential. Therefore we deposited the MnCat not on ITO, but on 1.5 $cm^2$ of glassy carbon of 100 µm thickness (HTW Hochtemperatur-Werkstoffe GmbH). Sample cells were constructed by gluing the glassy-carbon working electrodes to a 0.2 mm thick PVC sample holder with a 13 mm × 13 mm window. A loop of a 4.5 cm long platinum wire with diameter 0.3 mm served as counter electrode. The MnCat was deposited according to protocol-C (Fig. S1). The sample holders with the deposited MnCat were flushed several times with water and then dried in air. After that the sample holders were filled with Mn-free phosphate buffer (pH 7) and the MnCat was equilibrated at 1.35 V for 2 min. The duration of 2 min was chosen as a trade-off between achieving quasi steady-state currents and minimizing film dissolution. The potential between working and counter electrode was recorded. Subsequently, the reference electrode was removed from the setup and a power supply was set to the previously determined potential difference between working and counter electrode. Keeping the voltage between the working and counter electrode constant, the MnCat (together with the phosphate buffer) was rapidly frozen by immersion in liquid nitrogen; the electrodes were disconnected only after freezing. Notably, no change in the edge position was found between samples frozen according to this procedure and the samples deposited on ITO and frozen after drying (see Fig. S12b).

**E. Protocols for deposition of the catalytically active Mn oxides.** Three different protocols were used to electrodeposit catalytically active material: (A) in 0.1 M $MgSO_4$ solution, changing the potential stepwise between +1.4 V and +0.25 V; (B) in de-ionized water, changing the potential stepwise between +2.15 V and -0.75 V, and (C) in de-ionized water by cycling of potential between +2.15 V and -0.75 V (sweep rate 100 mV/s). All protocols involved 25 cycles with 29 × 2 seconds duration each (total deposition time around 25 min).

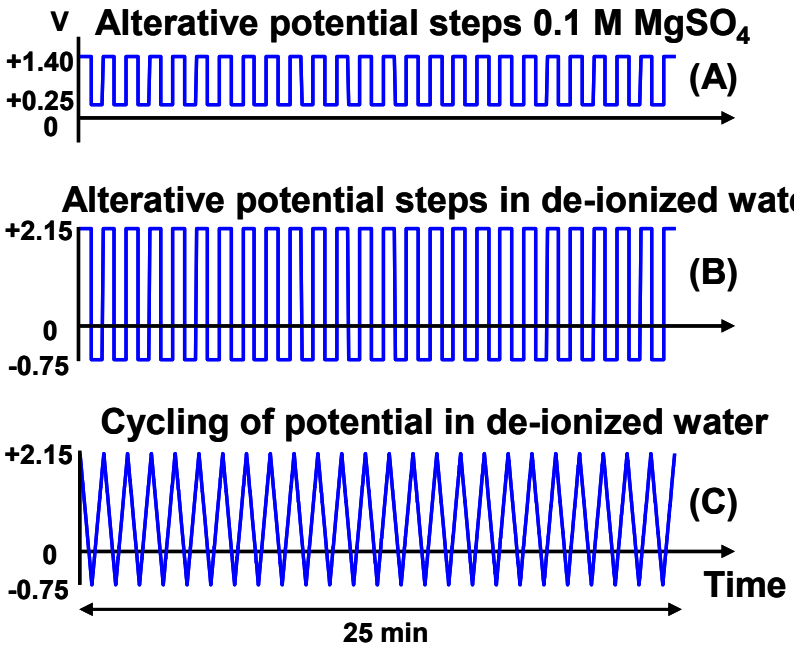


**Figure S1.**

Protocols used to deposit catalytically active Mn oxides. The number of steps (25) and the total duration (25 min) in all protocols was the same. No iR compensation was applied during the electrodeposition, resulting in a major difference between the indicated nominal potential and the real electrode potential (*vs*. NHE), in the absence of concentrated electrolyte (protocols-B and C). Film formation in de-ionized water using the potentials from protocol-A and applying 80% iR compensation also results in a formation of active MnCat.

## S-2. Mn oxides deposited at constant potentials and variable-potential methods

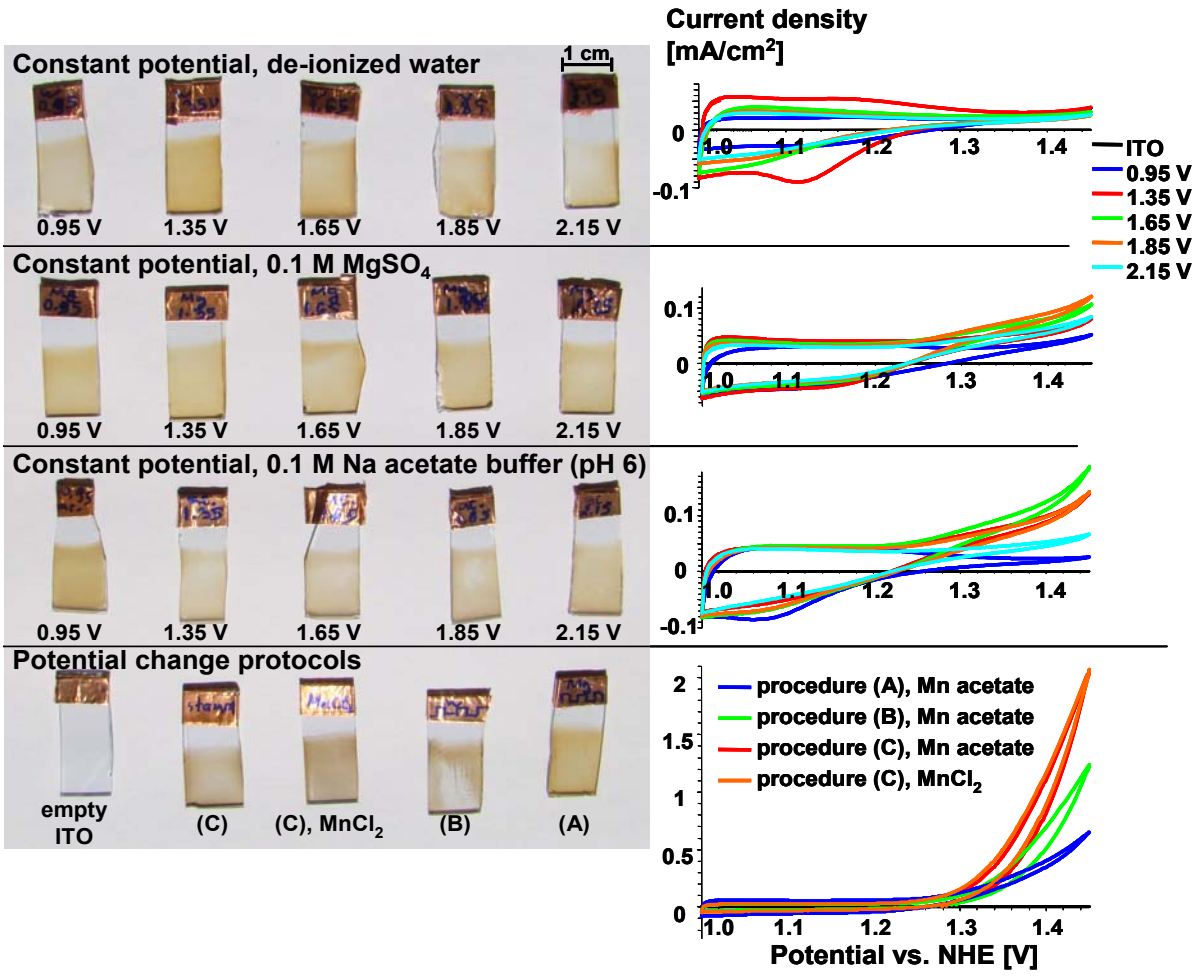


**Figure S2.**

*Left*: Mn oxide films deposited at constant potentials and by changing the potential in different electrolytes. 0.5 mM Mn(II) acetate tetrahydrate was added to each of the indicated electrolytes before the electrodeposition, except of the film shown in the lowest row in the middle where 0.5 mM $MnCl_2$ was used instead of Mn acetate. Typical pH of the non-buffered solutions was 6 - 6.5. Different constant potentials (in the range between 0.95 V and 2.15 V) were applied for 15 min or a potential change protocols A, B or C were used (see Fig. S1). After the deposition the films were rinsed with de-ionized water and dried on air for several hours before recording CVs in a Mn-free phosphate buffer.

*Right*: Cyclic voltammograms of electrodeposited Mn oxides (sweep rate 20 mV/s, second CV scan shown). All tests were performed in 0.1 M phosphate buffer which does not contain $Mn^{2+}$ ions. The ITO substrate tested under these conditions shows no significant current (shown as a black line which overlapps with the abscissa). We note that the scale for the last plot differs clearly from the scale used for the first three plots. Current densities are indicated; the current values were divided by the actual area of the electrode which was covered with Mn oxide.

## S-3. Electrodeposition of MnCat in de-ionized water by cycling of potential (according to protocol-C)

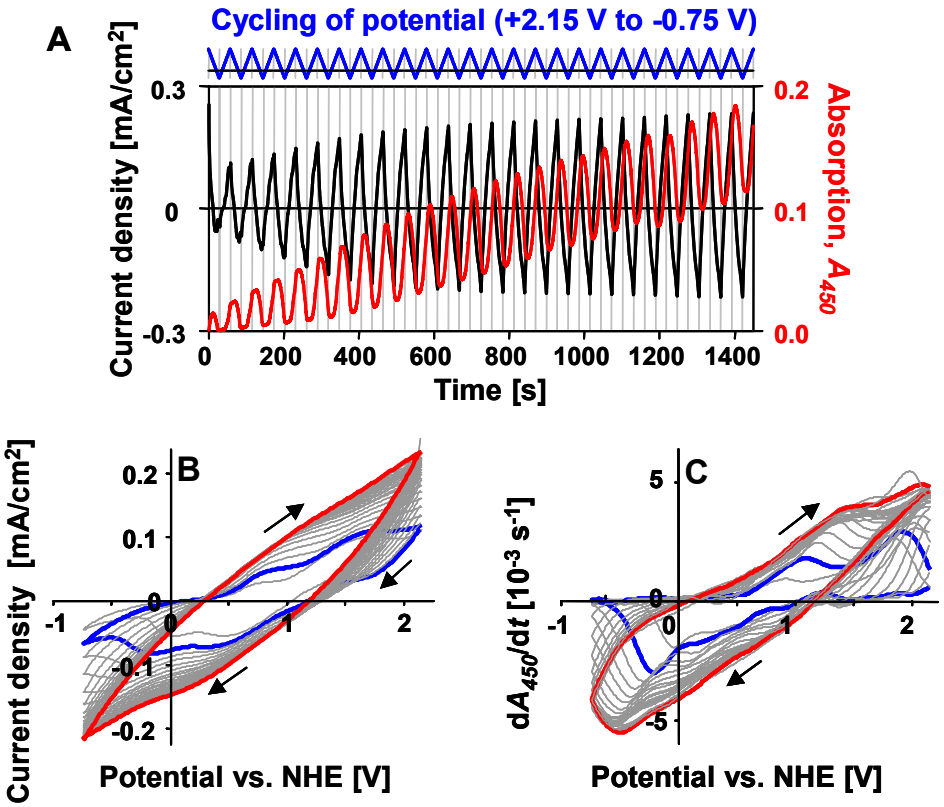


**Figure S3.**

Potentiostatic electrodeposition of a water-oxidizing Mn oxide (MnCat). The film was deposited at the working ITO electrode from aqueous $Mn^{2+}$ solution during 25 CV cycles of the potential (100 mV/s). (A) Potential protocol (blue line), current density (black line) and absorption at 450 nm (red line) during electrodeposition. (B) Current density during electrodeposition as a function of the applied potential. For increasing potential and at positive currents, two oxidation waves were detectable, which we tentatively assign to $Mn^{II}/Mn^{III}$ and $Mn^{III}/Mn^{IV}$ redox transitions, however this discussion in terms of electronically isolated Mn ions may be too simplistic. Upon decreasing the potential, the deposited $Mn^{IV}$ oxide was partially reduced but a net deposition of high-valent Mn ions is associated with each completed cycle. (C) First derivative ($dA/dt$) of the absorption detected at 450 nm. Similarity of the current density and $dA_{450}/dt$ traces implies that the current detected during the electrodeposition resulted mostly from oxidation state changes of the Mn ions. The current deviated from the absorption changes only at low negative potentials, where reduction of dissolved oxygen likely takes place, and at very high potentials, where water oxidation occurs. The second cycle in panels B and C is highlighted using blue color and the 25$^{th}$ cycle using red color.

## S-4. Electrodeposition of MnCat in de-ionized water by stepwise change of the potential (according to protocol-B)

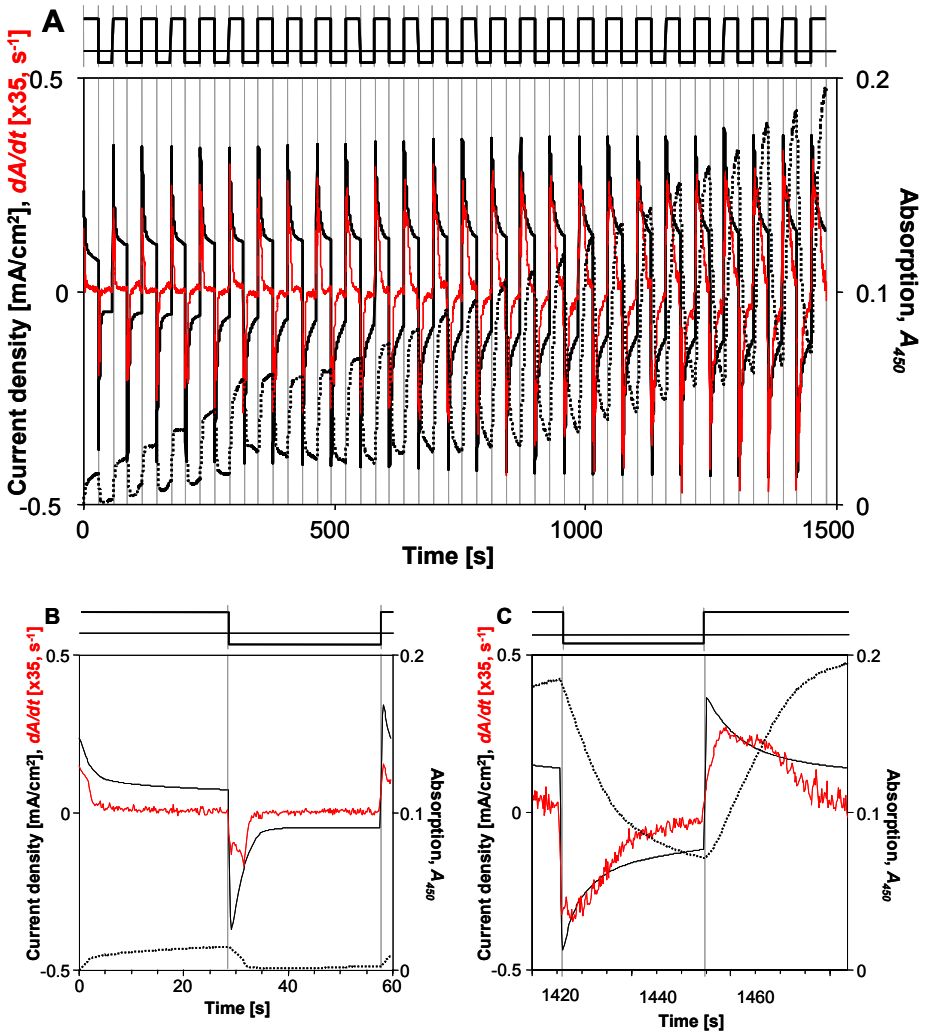


**Figure S4.**

The Mn oxide film was deposited during 25 cycles of alternating potential steps (2.15 V and -0.75 V vs NHE) of 29 s duration each (see **A**). The resulting film is an active catalyst for water oxidation. We note that using this protocol the film formed is not as homogenous as the film prepared during 25 CVs in the same potential range (as judged by visual inspection, Fig. S2). The current density during the electrodeposition (solid black line), the absorption (dotted black line), and the calculated derivative of the absorption (red line) are shown. The first two potential steps of the film formation in **B**; the last two potential steps are shown in **C**. Due to the absence of a concentrated electrolyte, the resistance between working and reference electrodes was high (4.1 kΩ), so that the actual electrode potential deviates significantly from the nominal potential of the working electrode.

## S-5. Electrochemical characterization of the MnCat

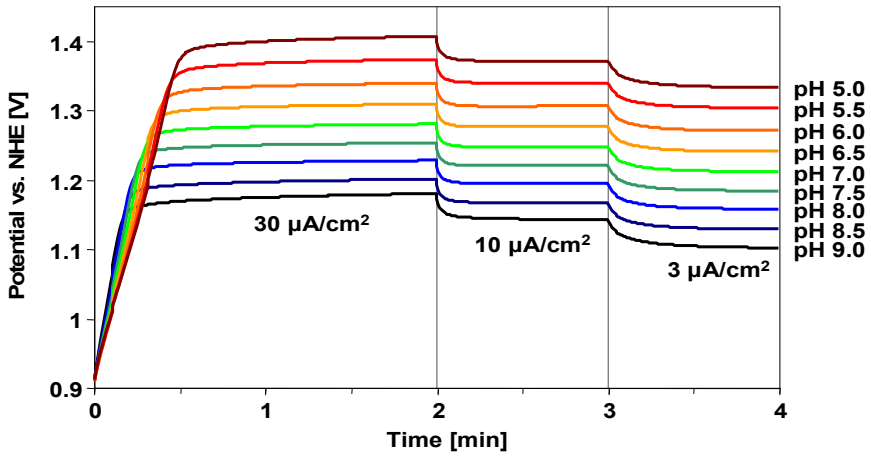


**Figure S5a.**

Chronopotentiometric measurements used to obtain the pH dependency shown in Figure 4A in the main text. Three current steps were used at each pH, starting at pH 9 and down to pH 5. Starting at pH 9, the desired pH was carefully adjusted with concentrated $H_3PO_4$ solution. The actual pH was permanently controlled by a pH-meter with the pH electrode close to the working electrode of the electrochemical cell (but galvanically fully isolated from the electrochemical experiment). For each step, the final value was taken for the pH-dependence plot of Fig. 4A.

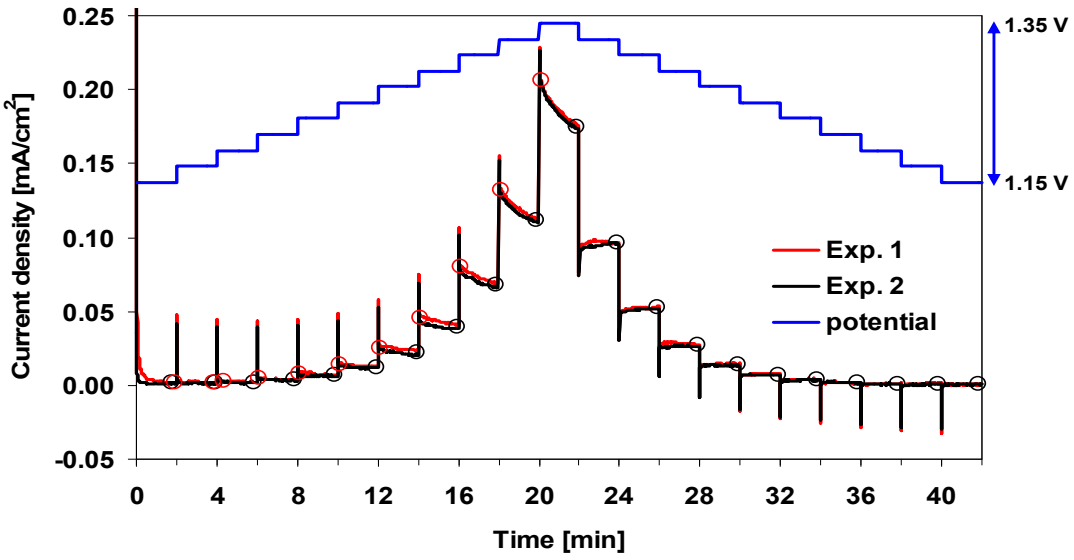


**Figure S5b.**

Chronoamperograms used for preparation of the Tafel plot in Figure 4B in the main text. Two MnCat films prepared independently (black and red line) were investigated applying different potentials (blue line), as shown in the plot. The current values were recorded at 10 ms resolution and averaged over 0.5 s. The solution was not stirred during the measurements.

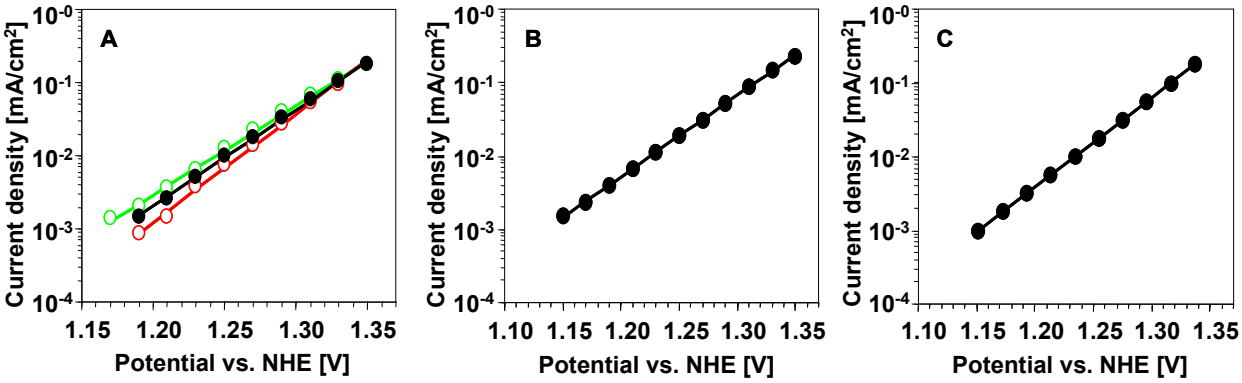


**Figure S5c.**

Tafel plots for the MnCat in 0.1 M $Mn^{2+}$-free phosphate buffer (pH 7, room temperature). The collection of optimal Tafel plot data is not trivial because a well-defined steady-state value is not reached even after an extended period of time. The time dependence of the current after changing the potential is determined not only double-layer recharging (very fast) but also by oxidation-state changes of the catalyst (within about 0.2 – 0.7 s), by mass-transport limitations (several minutes), and by catalyst dissolution (tens of minutes). As there is no simple way to obtain an optimal Tafel plot, we have used and compared several alternative approaches. We find that using different ways to establish a Tafel plot, we obtain Tafel slopes always close to 80 mV per decade (of the current density). The Tafel plots shown above were obtained as described in the following.

**(A)** Tafel plots prepared from the quasi steady-state levels reached 2 minutes after applying the potential step (black circles in Fig. S5b). Green – increasing potentials (82 mV/dec); red – decreasing potentials (67 mV/dec); black – average (76 mV/dec). The respective Tafel slope is given in parenthesis. The black curve is shown in Fig. 4B.

**(B)** Tafel plot prepared from the points taken after the spike related to the charging of the film (typically 0.2 – 0.7 s after applying the potential step, red circles in Fig. S5b). The Tafel slope is 90 mV/dec.

**(C)** Tafel plot obtained from a sequence of three 'slow CVs' (2 mV/s; between 0.9 and 1.45 V). The points in the plot were obtained from the second CV by averaging the current recorded during the cathodic and anodic scan. The Tafel slope is 82 mV/dec.

We note that also the pH-dependence data (Fig. S5a, Fig. 4A) imply a Tafel slope of about 80 mV per decade, irrespective of the pH.

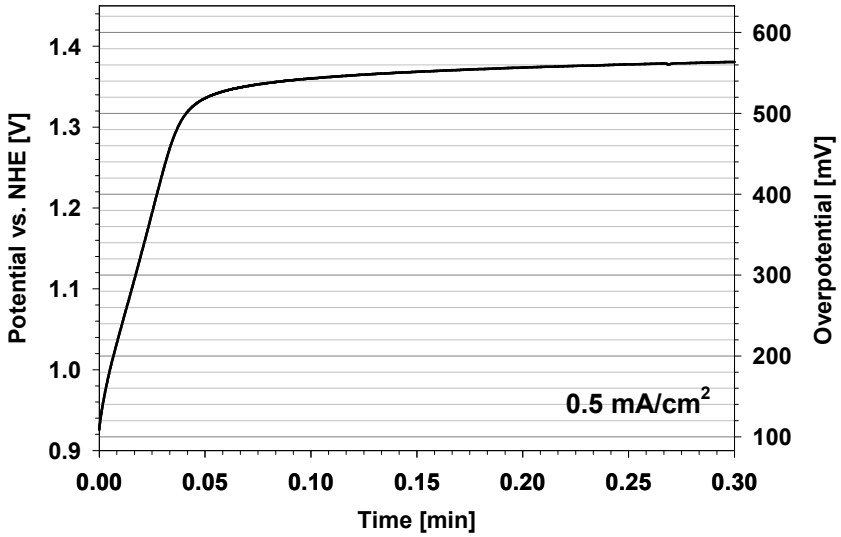


**Figure S5d.**

Chronopotentiometric measurements used to determine the overpotential for a current density of 0.5 mA/cm$^2$ (at pH 7, room temperature). The value at 18 s (0.3 min) after starting the chronopotentionmetric measurement is given in the main text.

## S-6. Oxygen evolution measurements

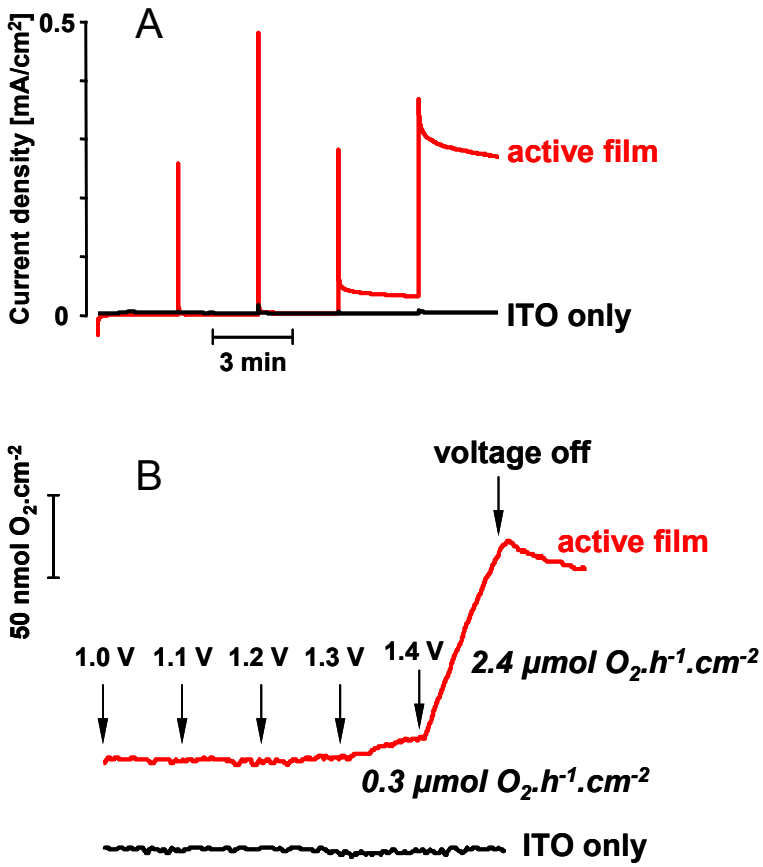


**Figure S6a.**

Oxygen evolution reflected (A) in the electrical current density and (B) detected with a Clark electrode. The indicated potentials (vs. NHE) were applied for 3 min (measurement in 0.1 M phosphate buffer, pH 7.0). The spikes in the current observed upon change of the potential are attributable to capacitive and oxidative charging of the MnCat. The slope of the $O_2$-signal of the Clark electrode corresponds to the indicated rate of dioxygen formation. For further details on the used electrodes systems and calibration, see S-1C. We cannot exclude that the detected rate of $O_2$ formation is diminished because of $O_2$ reduction at the platinum counter electrode. However, the high value calculated for the Faradaic efficiency suggests that the $O_2$ reduction by the counter electrode is negligibly small. (The current density at 1.4 V corresponds to an $O_2$-formation rate of 2.56 µm $h^{-1}cm^{-2}$.)

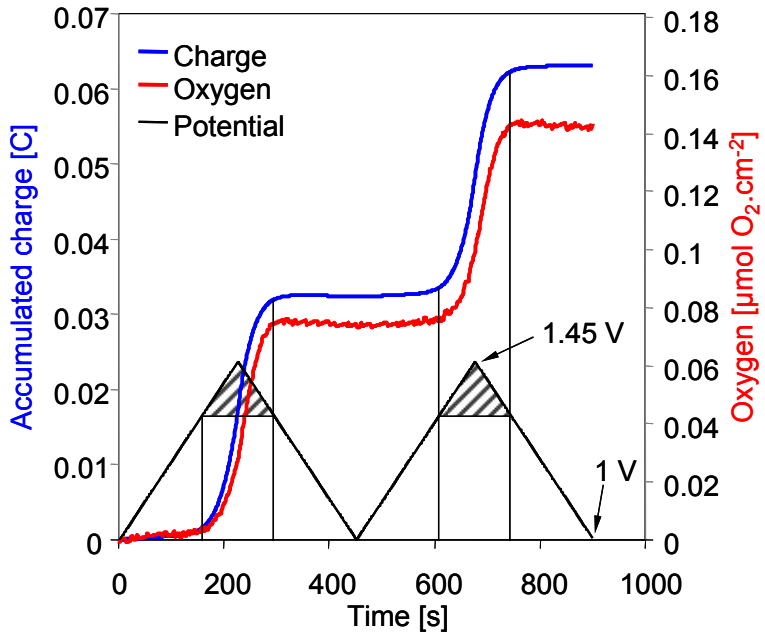


**Figure S6b.**

Oxygen detected with the Clark electrode during two CVs (from 1 V to 1.45 V) with a scan rate of 2 mV/s. The oxygen signal was corrected assuming a constant rate of $O_2$ consumption by the electrode. The simultaneously registered current was integrated to obtain the charge passed through the system. The right scale was chosen such that the charge (blue curve) would be mapped on the $O_2$-scale, if the Faradaic efficiency of the electrocatalysis were 100%. The minor mismatch of the red and the blue curve may indicate either that the Faradaic efficiency is slightly less than 100% or, more likely, the mismatch may result from the reduction of $O_2$ at the platinum counter electrode from the electrochemical setup which was in direct contact to the solution used for $O_2$ measurements with the Clark electrode.

## S-7. CV of the Mn film after annealing for 2 h at 90° C

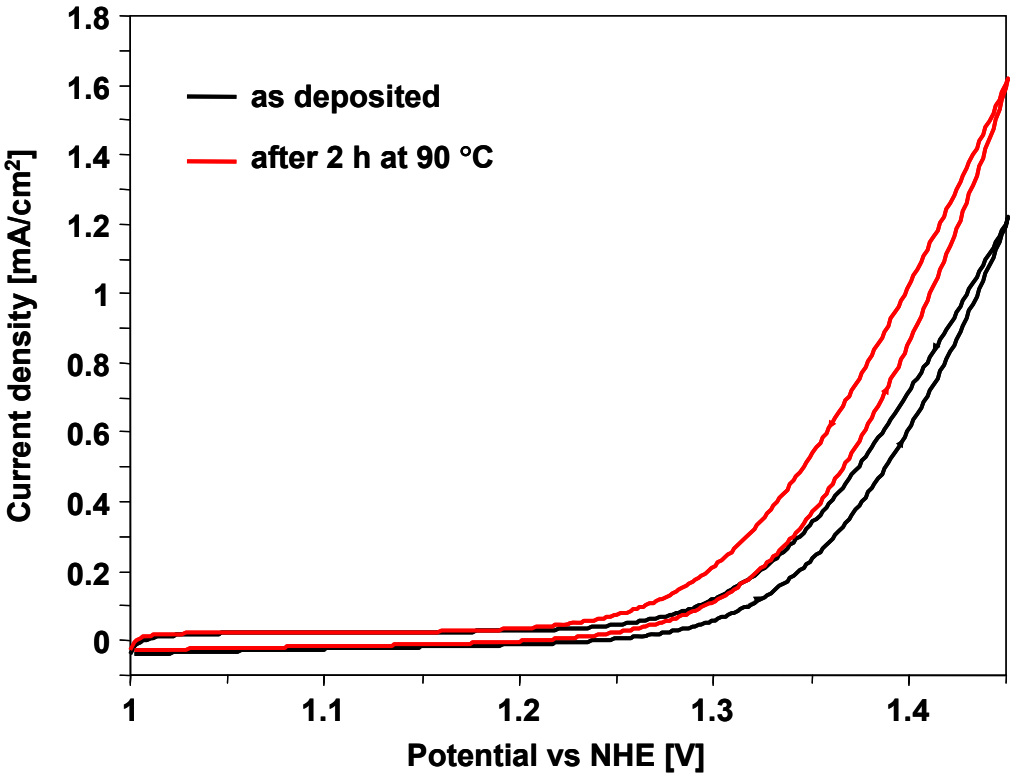


**Figure S7.**

Cyclic voltammograms (second scan) of the 'as-prepared' MnCat and after annealing at 90 °C for 2 h. The electrolyte was 0.1 M phosphate buffer (pH 7.0) with no $Mn^{2+}$ present and the scan rate was 20 mV/s. The annealing results in a moderate increase of the catalytic activity.

## S-8. Stability tests

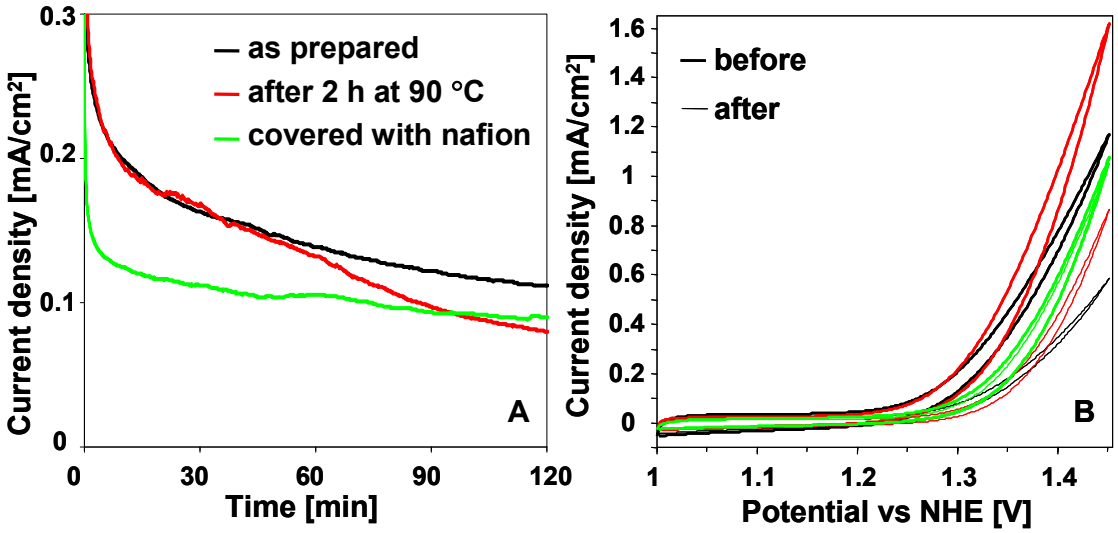


**Figure S8.**

**(A)** To test the stability of the Mn oxide films under working conditions, the films were kept for 2 h at 1.35 V in $Mn^{2+}$-free phosphate buffer (pH 7). In the first 0.5 – 1 s, the current decreases to a level of about 300 μA/cm$^2$ followed by a clearly slower decrease. Calculation of the turnover number (TON) for the time period on this plot gives value of 20 oxygen molecules per 1 Mn atoms. (The amount of produced dioxygen was calculated assuming 100% Faradaic efficiency.)

**(B)** CV tests (3 cycles) were performed before (thick lines) and after (thin lines) the 2 hours at 1.35 V (the second cycle is presented). The activity remains almost unaffected only if the Mn film is covered with thin layer of nafion (Nafion® perfluorated resin solution purchased from Aldrich was diluted 100 times with iso-propanol; the film was covered with a drop of this solution and heated for 2 h at 90 °C to allow the polymerization of the Nafion).

## S-9. Attempt to activate already deposited inactive Mn oxide

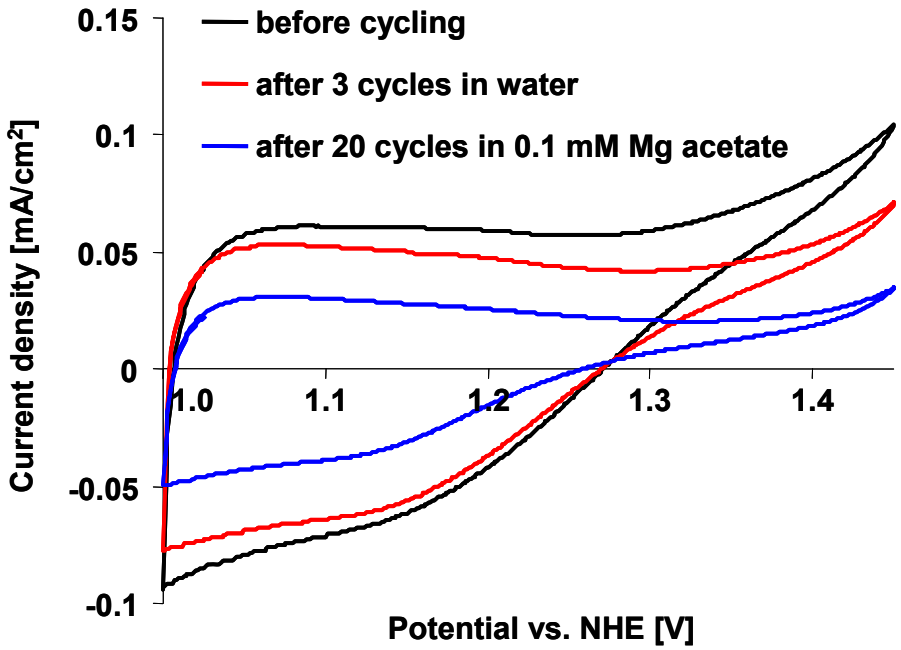


**Figure S9.**

Testing CVs of the inactive Mn oxide before and after cycling of the potential according to the protocol-C for deposition of an active MnCat. The stability tests (Fig. S8) and XAS measurements (Figs. S12B, D) showed that applying constant 1.35 V potential to the active MnCat does not lead to inactivation of the catalyst by structural transformation to an inactive Mn film. The assess whether cycling the voltage of a predeposited inactive film would induce catalytic activity we designed the following experiment: Catalytically inactive Mn oxide was deposited on ITO at 1.35 V in water for 15 min. After that the film was rinsed with de-ionized water and covered with Nafion as described in S-7 to prevent further dissolution of the deposited Mn. The CV test in 0.1 M phosphate buffer (pH 7) of the film covered with Nafion showed essentially no catalytic activity (black line). After this test the film was transferred in pure de-ionized water where cycling of voltage according to the protocol (C) for deposition of the MnCat were applied. After three cycles between -0.75 V and 2.15 V with sweep rate 100 mV/s, the film was tested again for catalytic activity in 0.1 M phosphate buffer (red line). As during the cycles in water no iR compensation was applied according to the protocol (C), and the uncompensated electrolyte resistance in pure water is even higher than in 0.1 M Mn acetate, used in the original protocol, we repeated the cycling procedure in water solution containing 0.5 mM Mg acetate to substitute the 0.5 mM Mn acetate. After 20 cycles between -0.75 V and 2.15 V with sweep rate 100 mV/s the test in phosphate buffer showed that the film is still inactive (the testing CV shown with blue line). We conclude that we can not induce catalytic activity in the pre-deposited inactive Mn oxides by applying potential cycling protocol.

## S-10. Additional SEM images – Mn oxides on glassy carbon

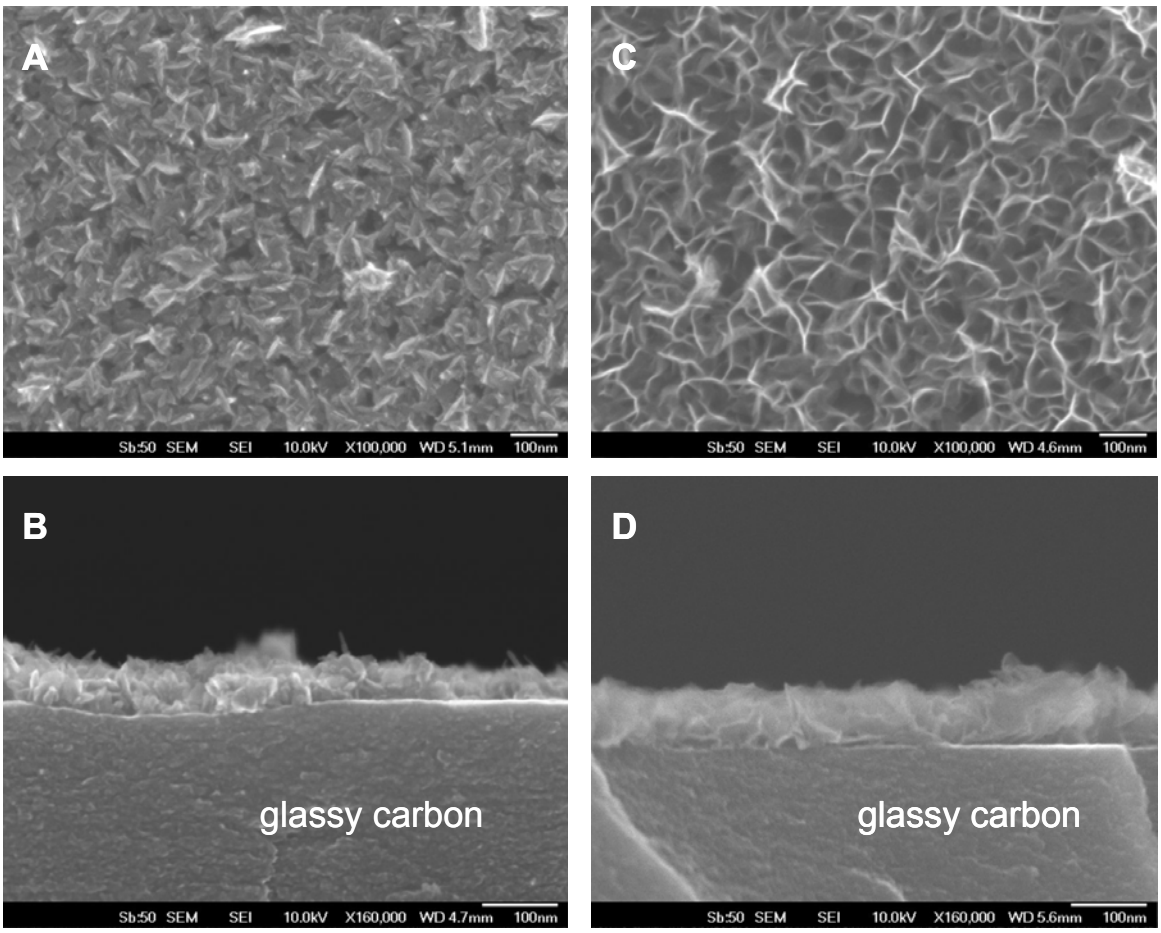


**Figure S10.**

SEM images from the active **(A, B)** and inactive **(C, D)** Mn oxides deposited on glassy carbon (instead of ITO). **A** and **C**, the top view; **B** and **D**, cross-section. The layer thickness is estimated to be approximately 20 nm.

## S-11. Elemental analysis by TXRF and EDX

*A. Total reflection X-ray fluorescence (TXRF)*

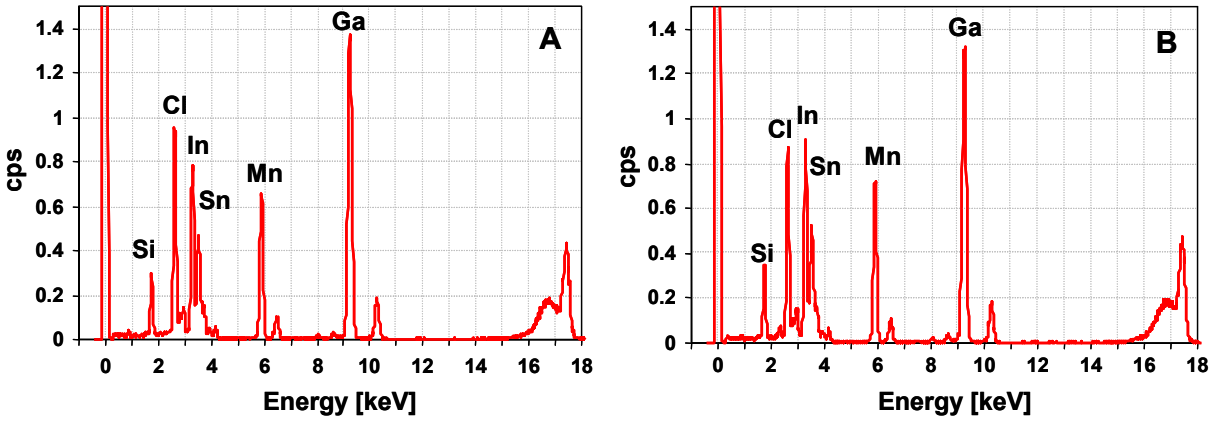


**Figure S11a.**

Typical TXRF histogram from the MnCat **(A)** and the inactive **(B)** Mn oxide. In the two oxides comparable amount of Mn were deposited, namely 80 ± 4 nmol.cm$^{-2}$ for the MnCat and 98 ± 4 nmol·cm$^{-2}$ for the inactive Mn oxide.

*B. Energy-dispersive X-ray analysis (EDX)*

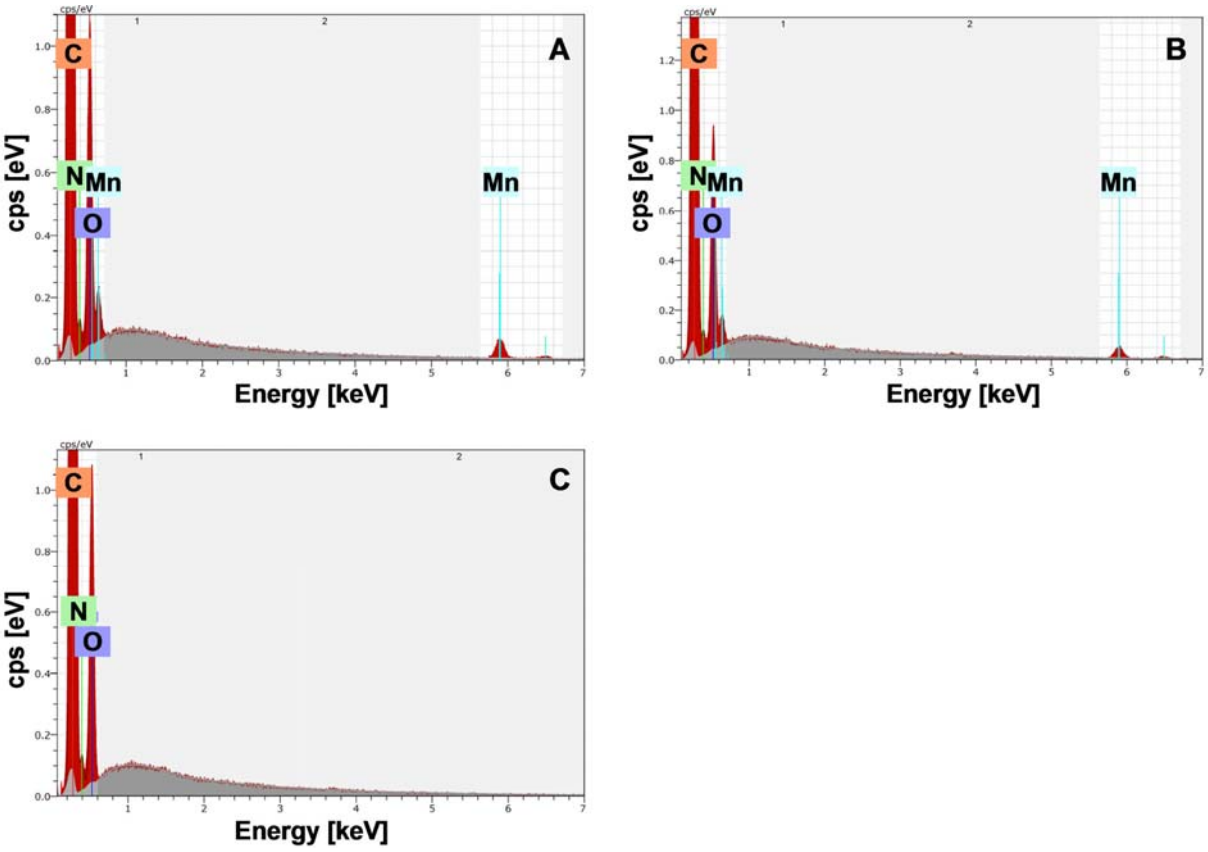


**Figure S11b.**

Typical EDX histogram (measured at 10 kV) for the active **(A)** and the inactive **(B)** Mn film deposited on glassy carbon (EDX histogram of the clean glassy carbon is shown in **C**). The glassy carbon was chosen as the Mn films deposited on ITO (i) do not form complete layers and (ii) In, Sn and O (from the ITO) and also Ca, Na, Mg and Br (from the glass support) were visible in the EDX. The EDX data confirms that manganese is the only detectable element which is deposited in both the MnCat and the inactive Mn oxide.

## S-12. Additional XAS data and analysis.

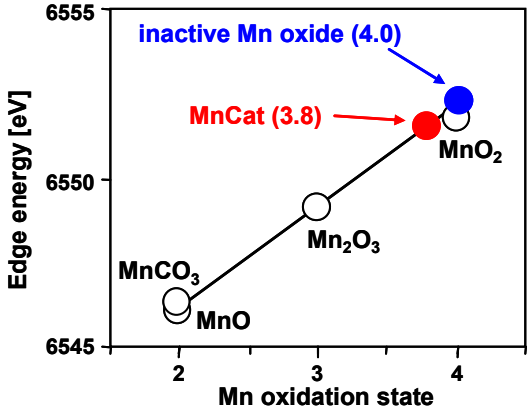


**Figure S12a.**

Relation between edge position and formal Mn oxidation state[7] for five reference compounds ($Mn^{II}O$, $Mn^{II}CO_3$, α-$Mn^{III}_2O_3$, and β-$Mn^{IV}O_2$, open circles). The mean oxidation states of the active Mn oxide film (around +3.8, red circle) and of the inactive Mn oxide (+4.0, blue circle) were estimated by means of the calibration line drawn for the edge positions of the reference Mn compounds.

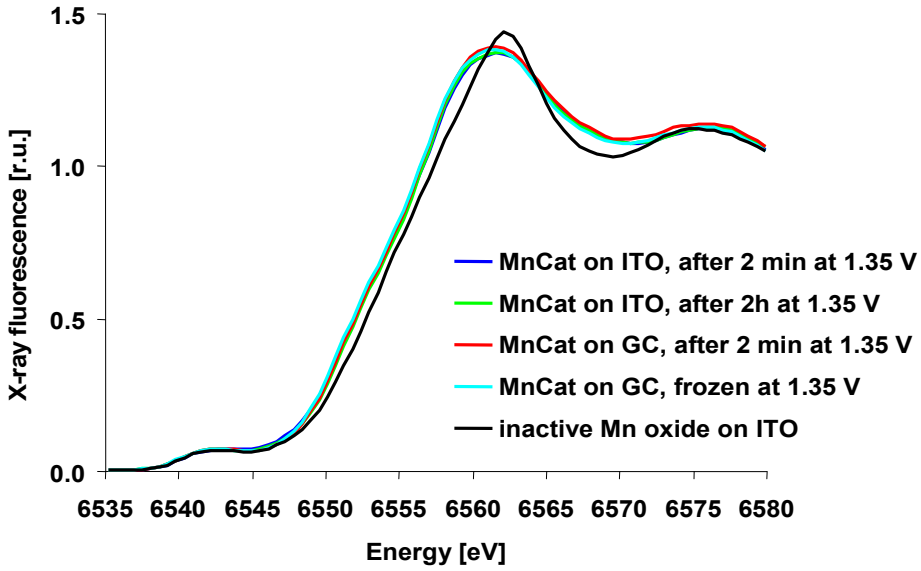


**Figure S12b.**

In addition to the XANES spectra of MnCat and inactive Mn oxide presented in the inset of Fig. 6, spectra of the MnCat after 2 h operation at 1.35 V in phosphate buffer and of MnCat deposited in glassy carbon (GC) and frozen under voltage applied as described S-1D are shown. All the spectra of the MnCat are very similar and consistently a show lower oxidation state of the Mn ions (ca. +3.8) than present the inactive Mn oxide (ca. +4.0).

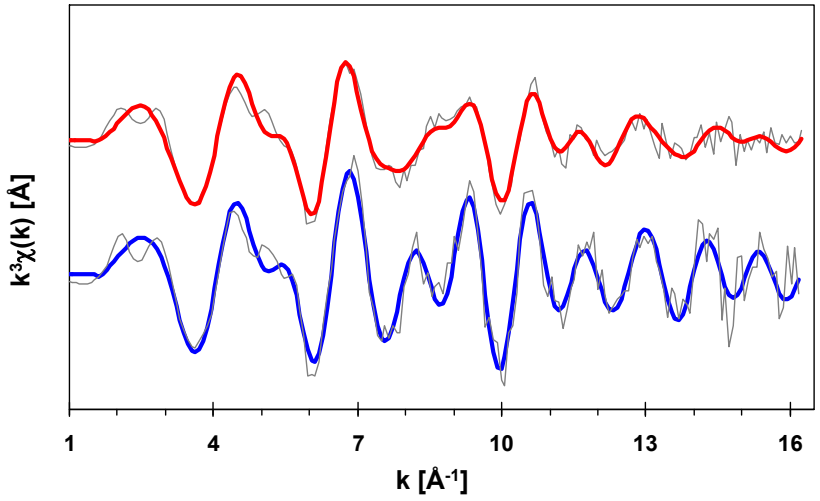


**Figure S12c.**

$k^3$-weighted extended-range experimental EXAFS spectra of the MnCat and inactive Mn oxide (thin gray lines) and simulation result (red line for MnCat, blue for the inactive Mn oxide). The fit parameters are given in Table 1 in the main text.

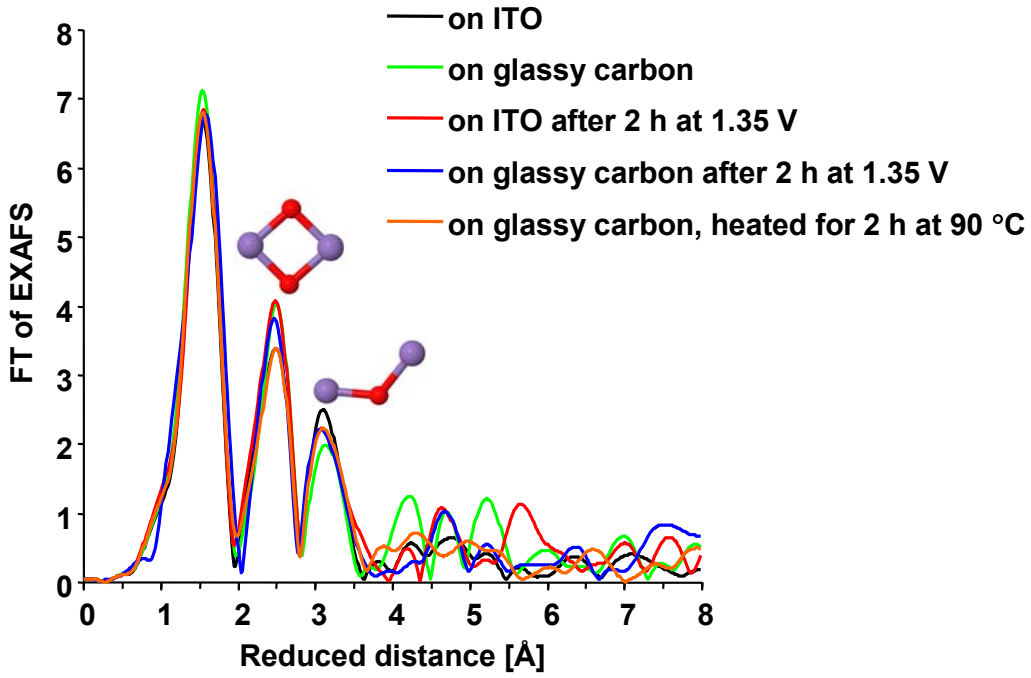


**Figure S12d.**

Fourier-transformed EXAFS spectra of active Mn film (MnCat) electrodeposited on ITO or glassy carbon and after operation for 2 h in phosphate buffer at pH 7. The spectrum of MnCat heated at 90 °C is also shown. The structure of the MnCat remains unchanged when 1.35 V are applied for a prolonged time period.

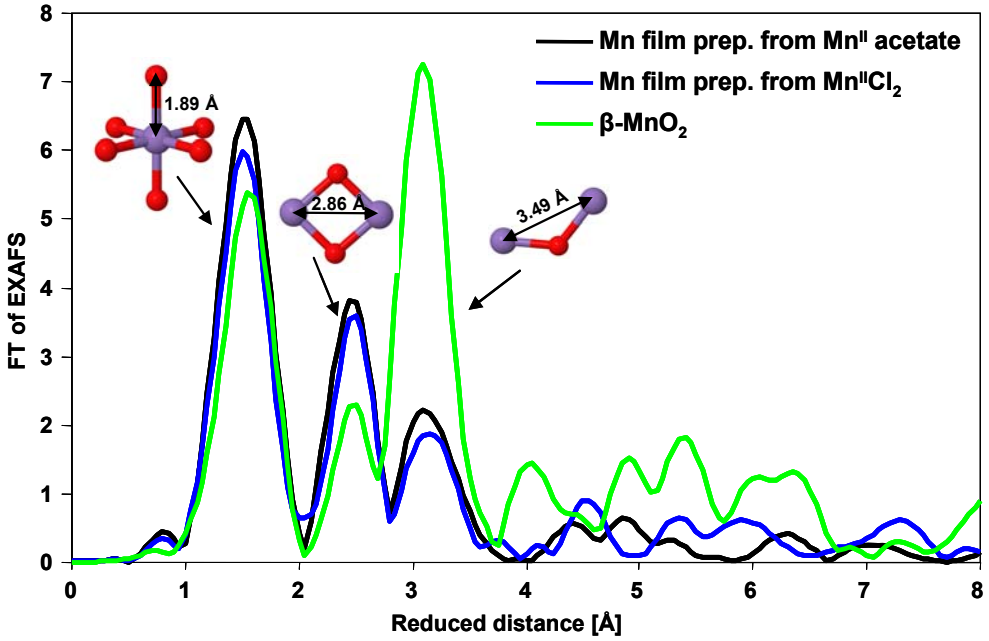


**Figure S12e.**

Fourier transformed EXAFS spectra of active Mn film (MnCat) electrodeposited in aqueous solution of 0.5 mM $Mn^{II}$ acetate or 0.5 mM $Mn^{II}Cl_2$. The XAS spectra of the Mn film prepared in $MnCl_2$ and in Mn acetate are essentially identical, with the third peak at 3.49 Å visible in both oxides. This excludes the carboxylate-bridging by acetate ligands as a possible explanation for the 3.49 Å Mn–Mn distance. The position of the third peak coincides well with the FT peak assignable to mono-μ-oxo bridged Mn atoms in β-$MnO_2$ (pirolusite).

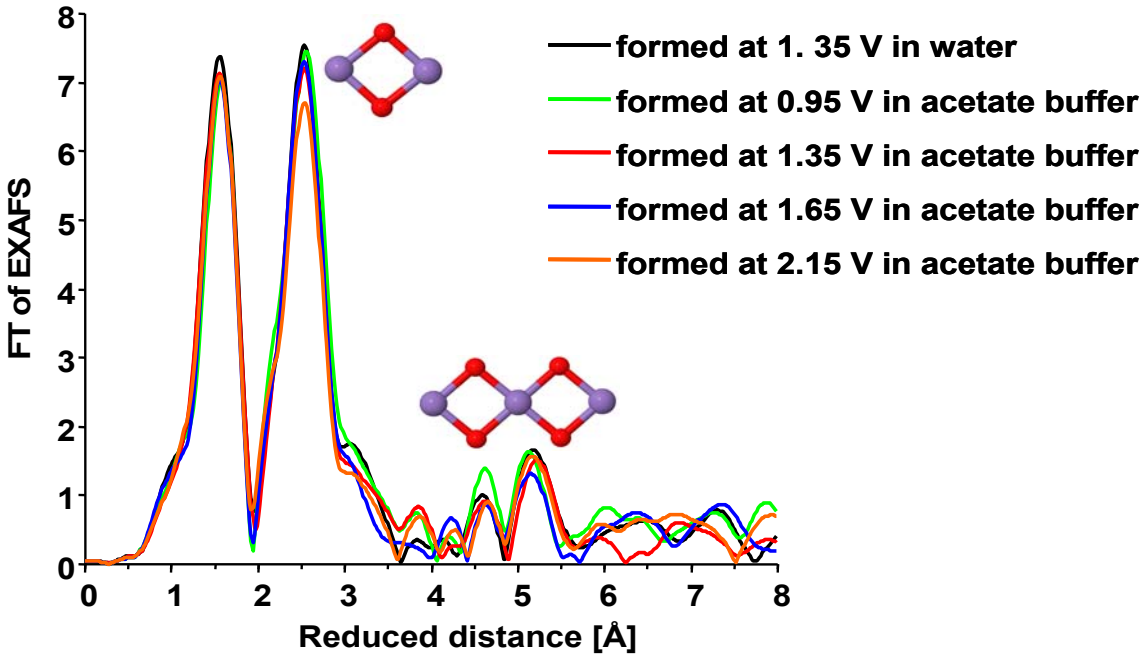


**Figure S12f.**

Fourier transformed EXAFS spectra of inactive Mn film electrodeposited on ITO under different constant potentials in water or in 0.1 M acetate buffer (pH 6).

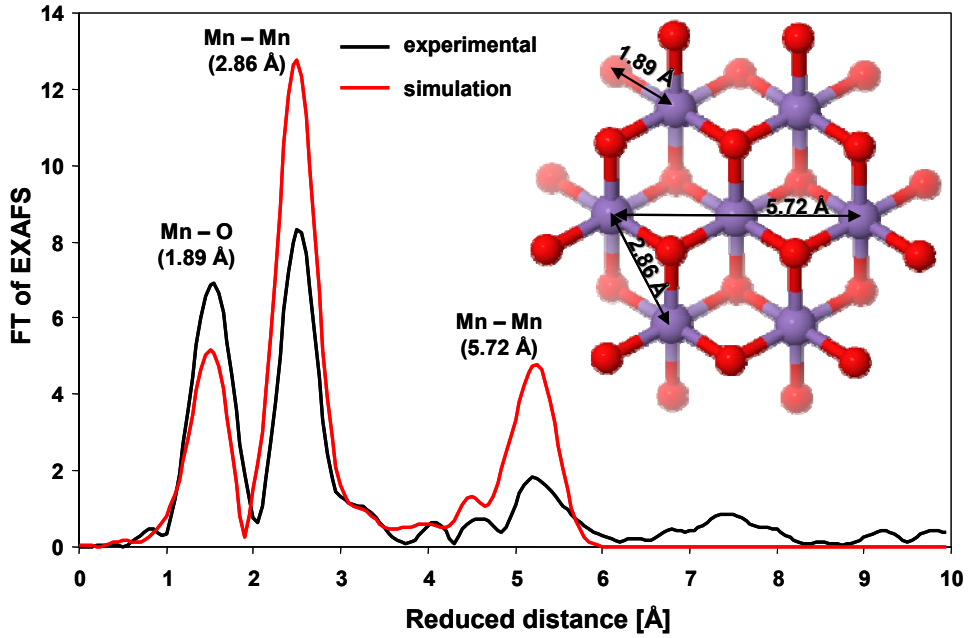


**Figure S12g.**

Fourier-transformed EXAFS spectra of the inactive Mn-oxide film (black line) electrodeposited in 0.5 mM $Mn^{II}$ acetate at a constant potential of 1.35 V (vs. NHE, for 15 min) and hypothetical spectra (red line) for a perfectly ordered Mn oxide. The spectrum was simulating using FEFF9[5-6] (including all relevant multiple scattering paths) for a perfectly ordered layer of octahedrally coordinated Mn ions; see inset, for a layer fragment used as a model. The peak corresponding to twice the distance of 2.86 Å (Mn–Mn distances of 5.72 Å) is clearly smaller in the experimental spectrum supporting the absence of perfect order in the electrodeposited oxide.

## References


1. M. W. Kanan and D. G. Nocera, *Science*, 2008, **321**, 1072-1075.
2. M. Dincă, Y. Surendranath and D. G. Nocera, *Proc. Natl. Acad. Sci. USA*, 2010, **107**, 10337-10341.
3. M. Risch, K. Klingan, J. Heidkamp, D. Ehrenberg, P. Chernev, I. Zaharieva and H. Dau, *Chem. Commun.*, 2011, **47**, 11912-11914.
4. M. Barra, M. Haumann, P. Loja, R. Krivanek, A. Grundmeier and H. Dau, *Biochemistry*, 2006, **45**, 14523-14532.
5. J. J. Rehr and R. C. Albers, *Rev. Mod. Phys.*, 2000, **72**, 621-654.
6. A. L. Ankudinov, B. Ravel, J. J. Rehr and S. D. Conradson, *Phys. Rev. B: Condens. Matter*, 1998, **58**, 7565-7576.
7. H. Dau, P. Liebisch and M. Haumann, *Anal. Bioanal. Chem.*, 2003, **376**, 562-583.